Supporting information

Pt-like hydrogen evolution on V_2O_5/$Ni(OH)_2$ electrocatalyst

Abhishek Meena, Miran Ha,* S. Selva Chandrasekaran, Siraj Sultan, Pandiarajan Thangavel, Ahmad M. Harzandi, Bhupendra Singh, Jitendra N. Tiwari* and Kwang S. Kim*

Center for Superfunctional Materials, Department of Chemistry, Ulsan National Institute of Science and Technology (UNIST), 50 UNIST-gil, Ulsan 44919, Korea

* To whom all correspondences should be addressed

Prof. S. Kwang S. Kim
Centre for Superfunctional Materials
Department of Chemistry
Ulsan National Institute of Science and Technology (UNIST)
Ulsan 44919, Korea)
Phone: +82-52-217-5410, Fax: +82-52-217-5419
*E-mail: wildflo2s@unist.ac.kr; jitendra@unist.ac.kr; kimks@unist.ac.kr
Homepage: http://csm.unist.ac.kr/kim/index.html

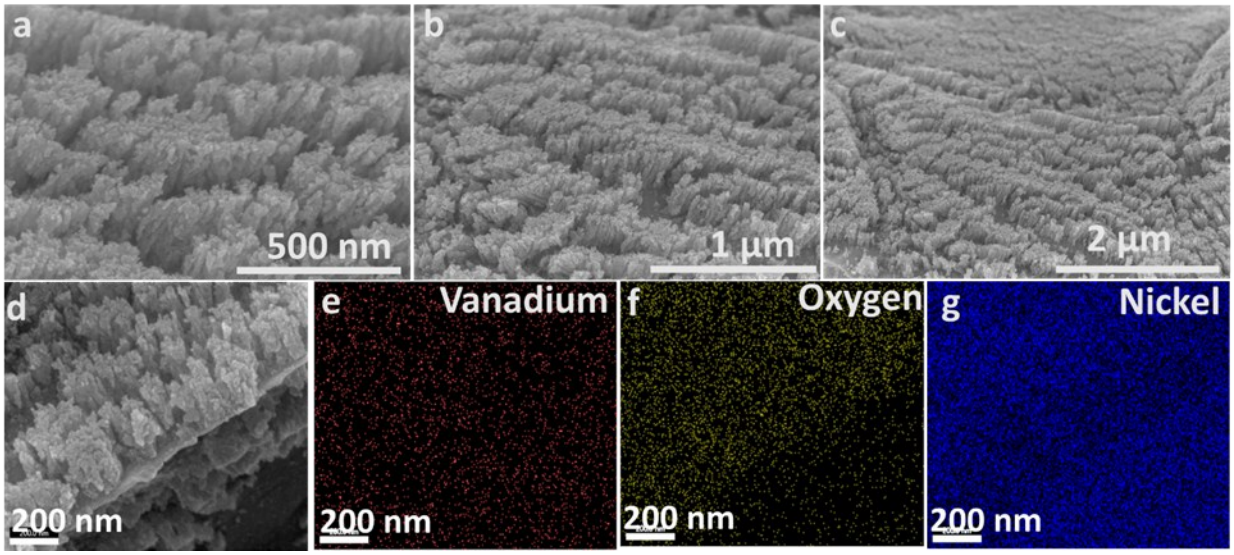

Fig. S1 SEM images at different magnification (a-c) and SEM–EDS elemental mapping of V, O and Ni (D-G) for V_2O_5/Ni(OH)$_2$@NF.

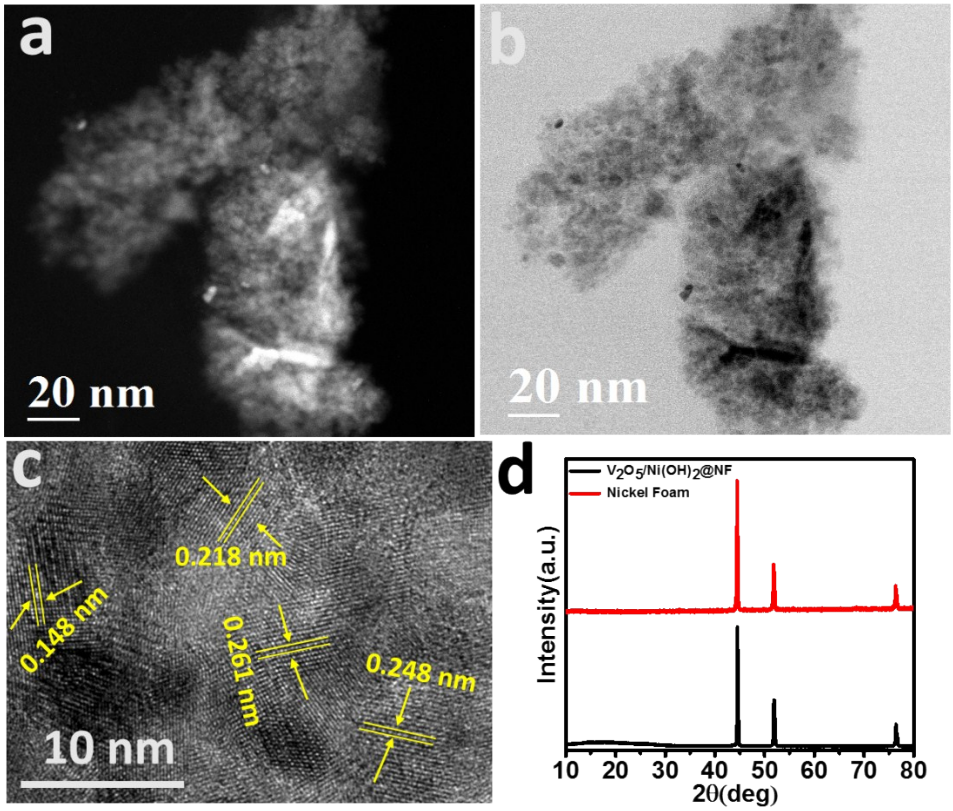

Fig. S2 (a) Dark-field STEM image, (b) bright-field STEM image, (c) HRTEM images and (d) XRD of V_2O_5/Ni(OH)$_2$@NF. It shows that the Ni(111) surface corresponding to the strong peak at 2θ = 45° in (d) is the most exposed surface on V_2O_5/Ni(OH)$_2$@NF as well as nickel foam.

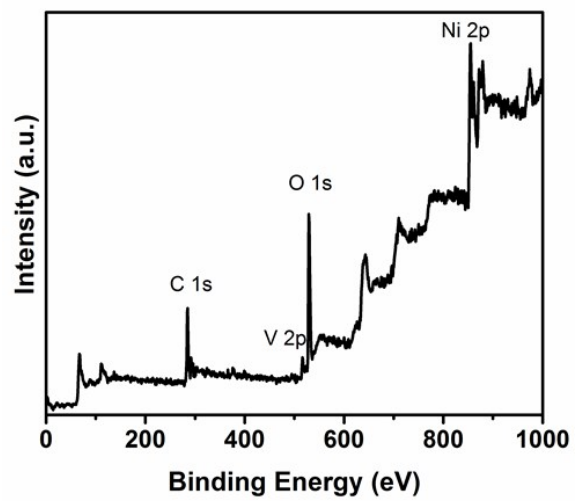

Fig. S3 XPS survey spectrum of the electrocatalyst V_2O_5/Ni(OH)$_2$@NF.

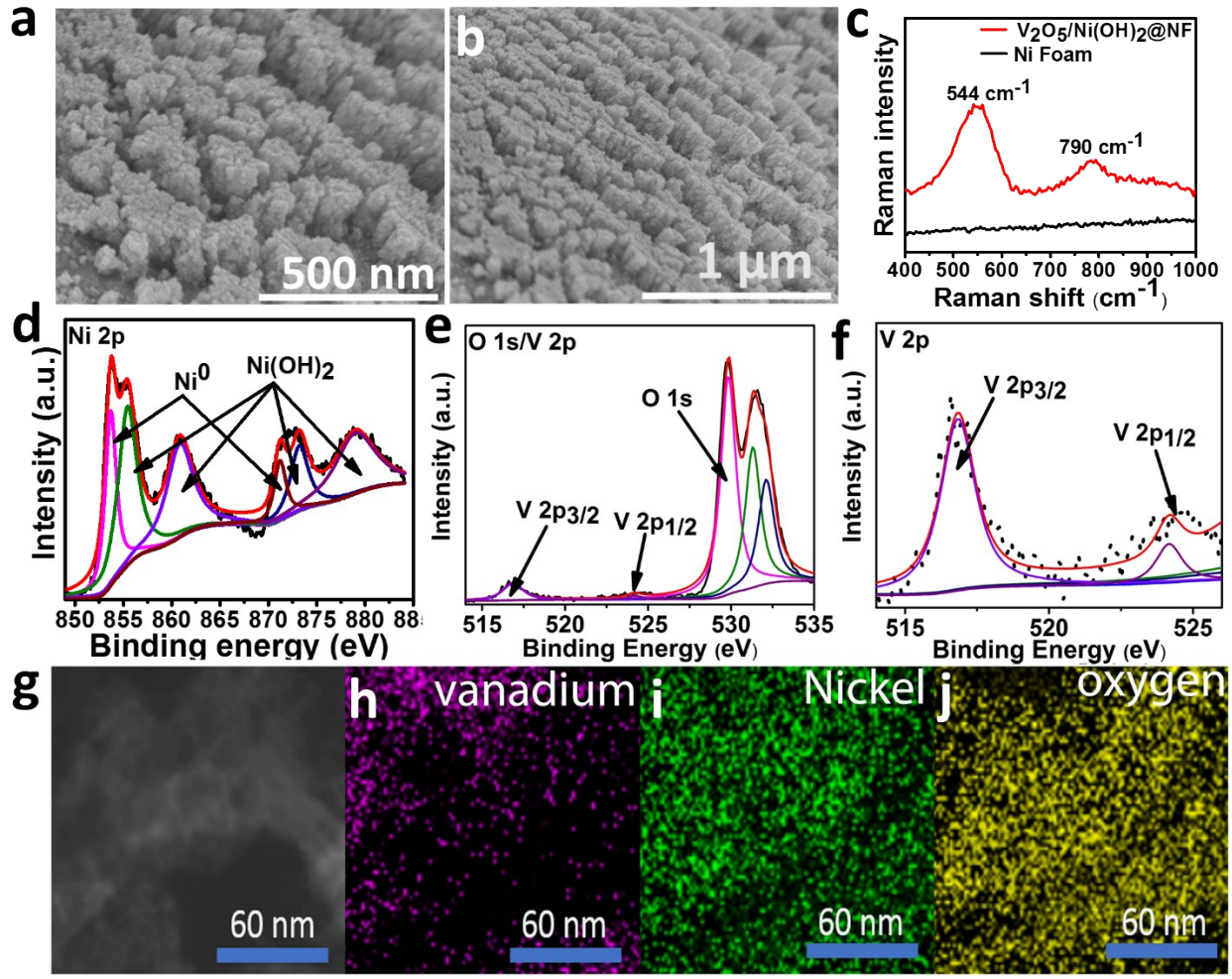

Fig. S4 Structural and compositional characterization of V_2O_5/Ni(OH)$_2$@NF after cyclic stability test. (a-b) FESEM image of V_2O_5/Ni(OH)$_2$@NF. (c) Raman spectrum of the V_2O_5/Ni(OH)$_2$@NF. High-resolution XPS spectra for constituent elements. (d-f) Ni 2p, O 1s, V

2p, and (f) zoom on V 2p core level spectra. (g-j) HRTEM images of V_2O_5/Ni(OH)$_2$@NF and the corresponding elemental mapping images of oxygen, vanadium, and nickel.

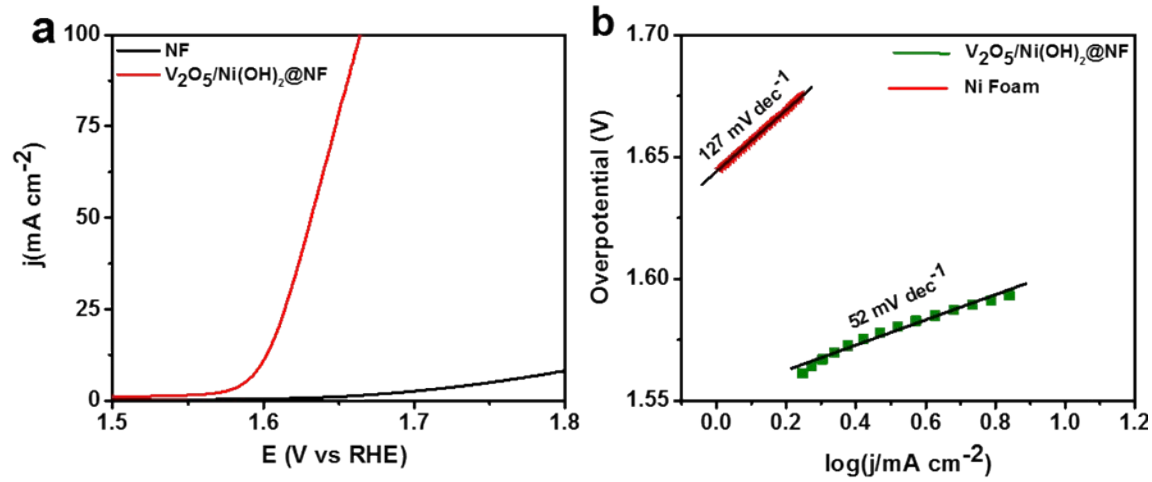

Fig. S5 OER polarization curves of V_2O_5/Ni(OH)$_2$@NF and bare NF in 1 M KOH. (a) Polarization curves of NF and V_2O_5/Ni(OH)$_2$@NF at a scan rate of 2mV s^{-1}. (b) Polarization curves derived Tafel plots of NF and V_2O_5/Ni(OH)$_2$@NF. As expected, the V_2O_5/Ni(OH)$_2$@NF exhibits much higher OER activity and lower Tafel slope than NF.

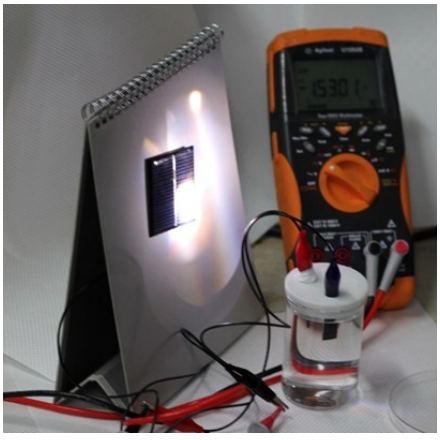

Fig. S6 Set up of water splitting by a solar panel (Two electrodes are connected to a solar panel and multi-meter).

Theoretical calculations

From the experimental findings, the theoretical model of V_2O_5/Ni(OH)$_2$@NF was designed to study HER properties using DFT. In order to make this structure, the (111) surface of Ni slab with three-layer thickness was cleaved from the FCC-Ni, and the 8×8 surface supercell was constructed in a hexagonal lattice (**Fig.** 6A) and it acted as a substrate of NF. At the top layer of Ni, the Ni(OH)$_2$ and V_2O_5 structures were deposited to construct the V_2O_5/Ni(OH)$_2$@Ni interfaces as shown in **Fig.** 6A. Before making this material, we carried out extensive studies of H adsorption property on (111) Ni-surface, NiO, Ni(OH)$_2$, and V_2O_5, separately (**Fig.** S7 to S11). With that, a piece of (010)V_2O_5 slab (breadth and width of 1.2 and 1.0 nm, respectively) was cleaved by considering a minimum energy configuration to deposit it on Ni surface along with optimization of the Ni(OH)$_2$ structure which leads to experimentally synthesized local structures such as V_2O_5@NF and Ni(OH)$_2$@NF (**Fig.** 6). In addition, we calculated the band structure of Ni(OH)$_2$ including various types of hydrogen coverage using the PBE+U method (U=6.2 eV for Ni) (**Fig.** S13).

In the synthesized V_2O_5/Ni(OH)$_2$@Ni, V_2O_5 was found in orthorhombic structure with P_{mmn} (Space group No. 59), and this structure was optimized using DFT calculations. The obtained lattice constant (a = 11.52 Å, b = 4.378 Å, and c = 3.527 Å) matches well with experiment (a = 11.51 Å, b = 4.37 Å, and c = 3.56 Å). The optimized structure of V_2O_5 is cleaved along the (100), (010), and (001) facets to calculate the surface energy. Here, $\gamma = \frac{E_{surf} - n \times E_{bulk}}{2A}$ is defined, where E_{sur}, E_{bulk}, and n are the ground state energy of cleaved structure, the single formula unit of bulk structure, and the number of formula units in the cleaved structure, respectively. The calculated γ for the (100), (010), and (001) surfaces are 0.23, 0.17, and 0.41 eV/Å^2, respectively. It expresses that the (010) surface stands energetically in favor of forming stable structure. Higher index facets tend to be less stable and the hydrogen adsorption energies on these less stable surfaces tend to be stronger [Z. Quan, Y. Wang, J. Fang, *Acc. Chem. Res.* 2013, **46**, 191-202]. Indeed, the ΔG_{H^*} on O atoms of V_2O_5 (001) and V_2O_5 (310) were too strong (<-0.6 eV), which makes them inactive surface for HER. We easily expect that any higher index surfaces of V_2O_5 would be inactive (Fig. S7, Fig. S8). Similarly, it is expected that any higher index surfaces of nickel foam would not be active.

The (010) surface of V_2O_5 with two atomic layer thickness (0.9 nm), as shown in **Fig.** S7 (a), was undertaken to study the HER activity. Four different sites of H binding at the top of the slab are represented in **Figs.** S7 (a). With respect to the coordination number of oxygen atoms at the surface, four active sites are distinguished. Sites S_1, S_2, and S_3 are oxygen atoms with coordination numbers, of one, two, and three, respectively, while S_4 is a surface V site. The calculated ΔG_{H^*} values for all four sites show that S_1 and S_2 tend to adsorb H, while S_3 and S_4 (a more positive value which is not shown in the Fig. S7 (c)) are ready to desorb H. Among these four sites, S_2 is highly active with near-zero ΔG_{H^*} of -0.14 eV, and the next active site is S_1 with ΔG_{H^*} of -0.32 eV. The same calculations were repeated for three atomic-layer-thick (010) surface slab (1.38 nm) and the obtained ΔG_{H^*} at S_1 and S_2 are -0.31 and -0.15 eV, respectively. This verifies the consistency in the calculations. In addition, (001) surface of V_2O_5 which was analyzed from TEM was also considered to calculate ΔG_{H^*} on three different O atom sites (S_5-S_7) and one V atom site (S_8) of surface (Figs. S7 (b)). H atom on S_8 atom was optimized to be on S_6 site. The calculated ΔG_{H^*} values for S_5-S_7 sites tend to adsorb H strongly and they are shown in Fig. S7 (c) also.

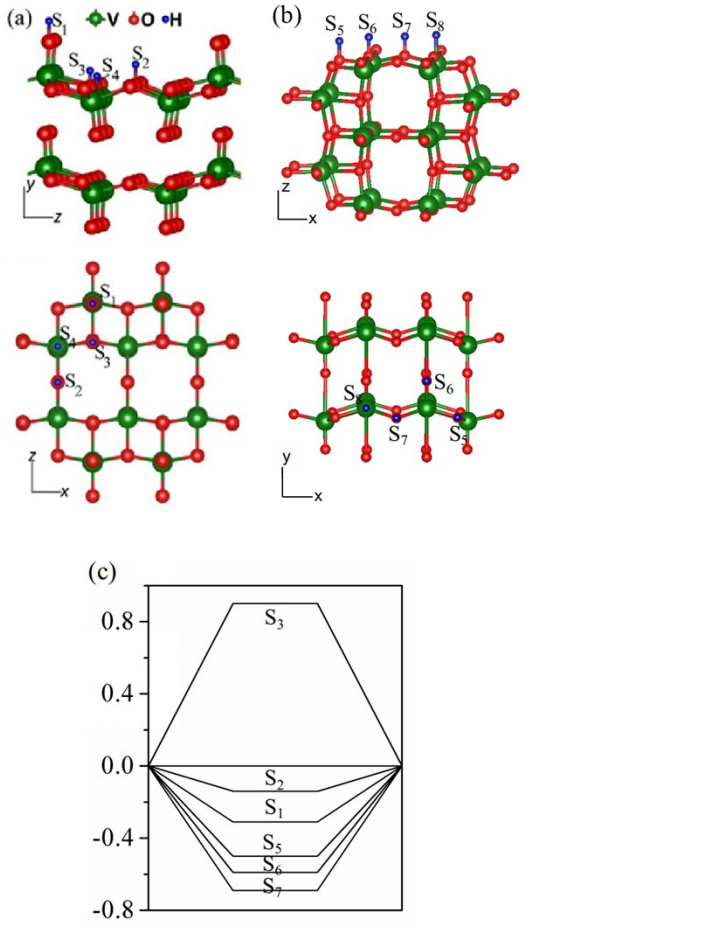

Fig. S7 Ball and stick models of the V_2O_5(010) and V_2O_5(001) surface of V_2O_5 slab: (a) top and side views of (010), and (b) top and side views of (001). The four different H adsorption sites are indicated by numbers 1 to 8. (c) H-adsorption Free energy (ΔG_{H^*}) profile for hydrogen adsorption sites S_1-S_3 in the (010) surface and S_5-S_7 in the (001) surface (the high ΔG_{H^*} value at S_4 =1.2 eV is not drawn here).

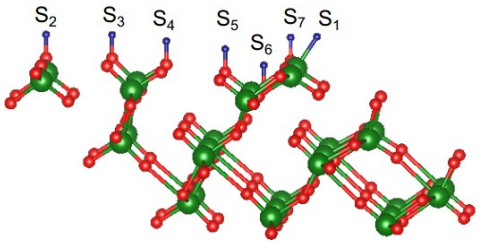

Site	ΔG_{H^*} (eV)
S_1 (V)	1.01
S_2 (O)	-1.98
S_3 (O)	-1.95
S_4 (O)	-2.13
S_5 (O)	-2.46
S_6 (O)	0.34
S_7 (O)	-1.11

Fig. S8 Ball and stick models of the V_2O_5(310) surface on V_2O_5 slab as a side view and the free energies (ΔG_{H^*}) at seven different H adsorption sites denoted as S_1-S_7. All sites give large ΔG_{H^*} except for only S_6 which is still not small.

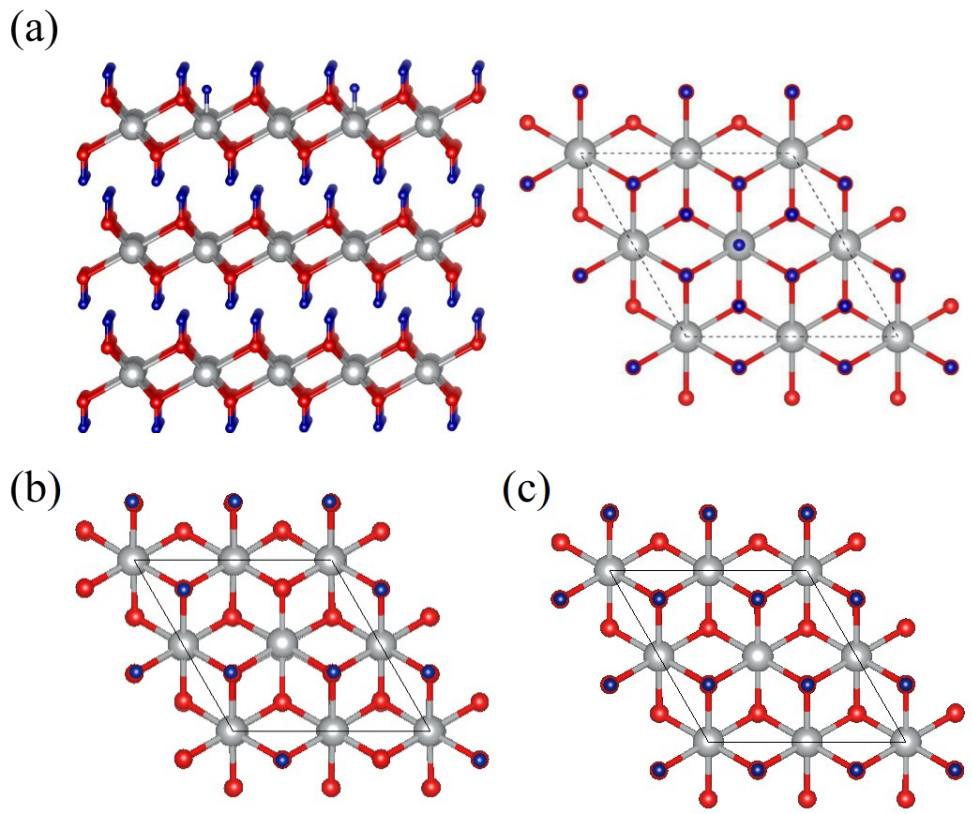

Fig. S9 Ball and stick models of side and top views of (a) H adsorbed on a surface Ni atom of $Ni(OH)_2$, (b) H adsorbed on a surface O atom of $Ni(OH)_2$-½H_d (i.e., $NiOH(OH_{1.75})$) and (c) H adsorbed on a surface O atom of $Ni(OH)_2$-¼H_d (i.e., $NiOH(OH_{0.75})$) with three layers thickness. Blue, red, and grey colors denote H, O, and Ni atoms, respectively. From the optimized bulk structure of $Ni(OH)_2$, a surface with 2×2 supercell along [100] crystallographic direction is cleaved and the three layers thick surface slab is modelled as shown in the Fig.. The H atom is attached on the Ni atom. The calculated H adsorption energy is 0.843 eV, which was not changed substantially when the thickness is reduced from three layers to one layer. Therefore, a piece of one layer thick $Ni(OH)_2$ is deposited on Ni surface for $V_2O_5/Ni(OH)_2/Ni$.

Fig. S10 Ball and stick models of side and top view of NiO(111) with a 4×4 supercell. Red and grey colors indicate O and Ni atoms, respectively.

The optimized structure of NiO is cleaved in (111) plane with 5L-thickness. The bottom surface is terminated with Ni atoms and it is kept fixed in order to achieve the bulk nature. Then, the top surface terminated with O atoms, which are allowed to relax and find the optimized structure. In this structure, there are two different H adsorption sites of Ni and O with H adsorption energies of -1.15 and -0.72 eV, respectively. The calculated values are very close to the values in a previous work.[5]

Fig. S11 Ball and stick models of Ni(111) surface. The optimized fcc Ni is cleaved along the (111) plane and a 4×4 supercell with 5 layers thick surface slab is constructed. In this surface, three different H adsorption sites are available on Ni atom (H bonded with one Ni atom), Ni-Ni bonding site (H bonded with two Ni atoms), and fcc site (H bonded with three Ni atoms). Among three sites, fcc site is energetically more stable and it produces adsorption energy of -0.535 eV.

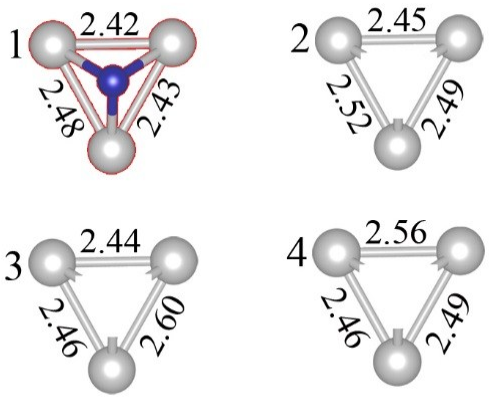

Fig. S12.Modified Ni-Ni bond lengths (in Å) at various H adsorption sites shown in Fig. 6A. (1) modified NF-surface, (2) $Ni(OH)_2$@Ni interface, (3) between V_2O_5@Ni and $Ni(OH)_2$@Ni, and (4) V_2O_5@Ni. The original Ni-Ni bond length at the pristine Ni-surface is 2.50 Å.

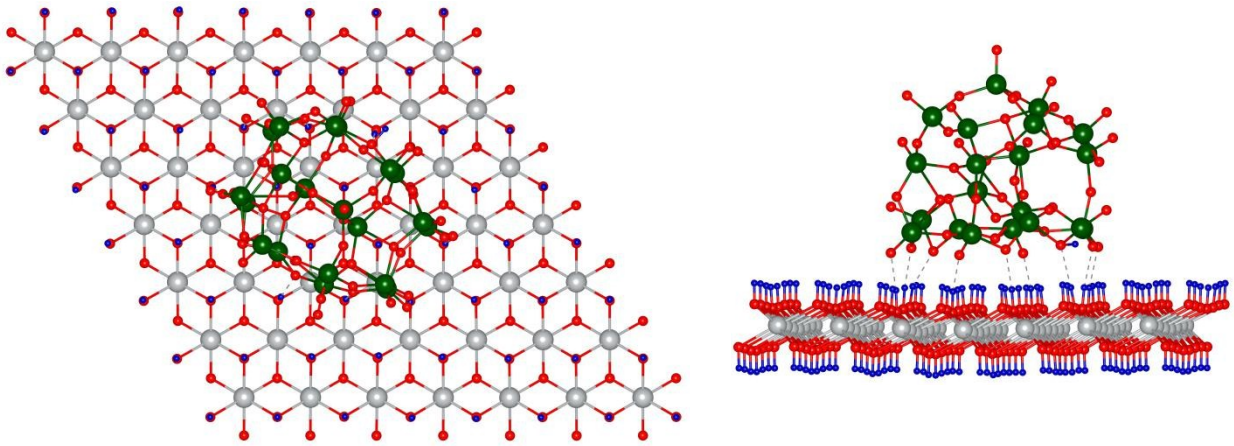

Fig. S13 V_2O_5@$Ni(OH)_2$ with H adsorption site at the interface. (a) Top view. (b) Side view (H: blue, O: red, V: green, Ni: light black).

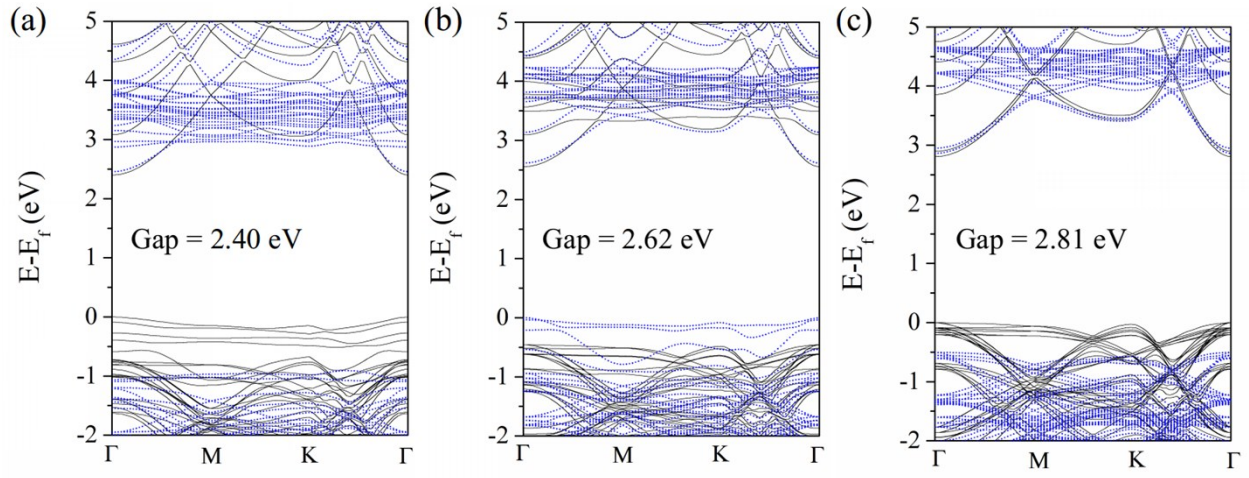

Fig. S14 Band structure of 2 bottom layers of $Ni(OH)_2$ and 1 top layer of (a) $Ni(OH)_2$-½H_d, (b) $Ni(OH)_2$-¼H_d, and (c) $Ni(OH)_2$. (The black solid lines and blue dashed lines in the band structures images represent the spin up bands and spin down bands, respectively). The structure with 3 layers of pure $Ni(OH)_2$ shows a high band gap of 2.81 eV. This value increases to ~5 eV towards the experimental value of 4 eV when GW calculation is performed. If H atoms are not fully covered on the surface of $Ni(OH)_2$, the band gap becomes smaller than that on its pure state.

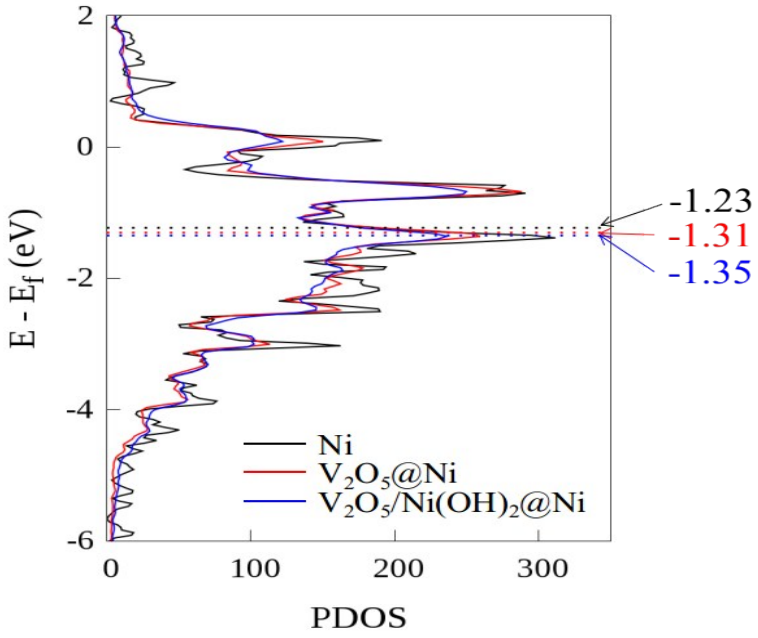

Fig. S15 Projected density of states (PDOS) (solid lines) and d-band center relative to fermi energy (ε_d-ε_F, dotted lines) of Ni top surface in pristine Ni, V_2O_5/Ni, and V_2O_5/Ni$(OH)_2$@Ni.

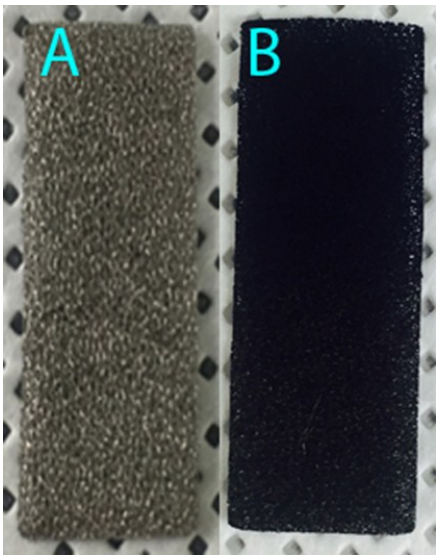

Fig. S16 Images of the electrode surface of V_2O_5/Ni$(OH)_2$@NF (a) before and (b) after the hydrothermal process. The color of NF changes from gray to black. This color change suggests

that the V_2O_5/$Ni(OH)_2$@NF particles are uniformly coated on NF and no uncoated portion is left on NF.

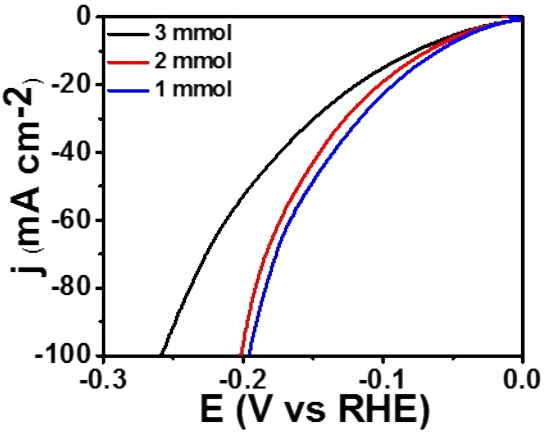

Fig. S17 Electrocatalytic HER activity of V_2O_5/$Ni(OH)_2$@NF catalysts synthesized with different precursor concentrations (NH_4VO_3).

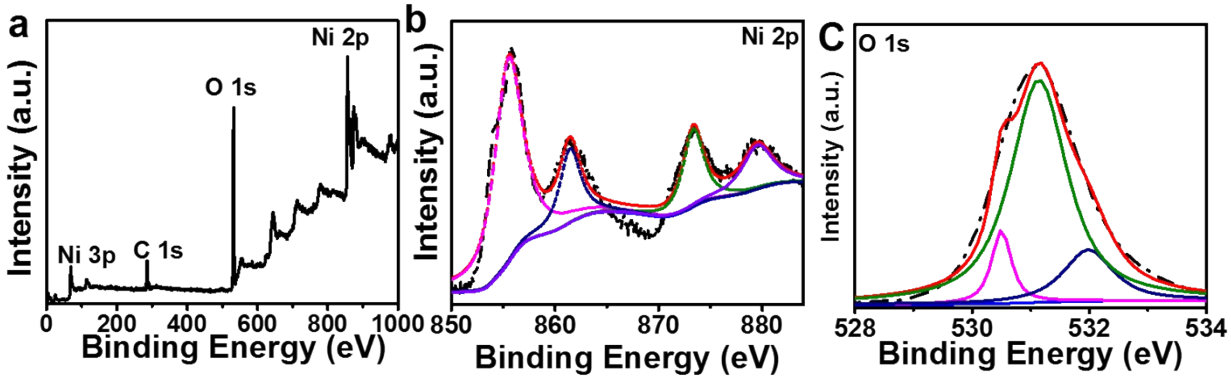

Fig. S18 The XPS survey scans of $Ni(OH)_2$@NF electrode (A), the corresponding Ni 2p (B) and O 1s (C) core level spectra. The Ni 2p spectrum shows two major peaks at 855.72 and 873.38eV, corresponding to Ni $2p_{3/2}$ and Ni $2p_{1/2}$, respectively, with a spin-energy separation of 17.6 eV, which is a characteristic signature of Ni^{2+} of $Ni(OH)_2$. Two shake up satellites peaks of Ni $2p_{3/2}$ and Ni $2p_{1/2}$ was located at around at 861.55 eV and 879.67 eV, respectively. The high resolution spectrum of O 1s contains a peak at 530.50 eV which usually is attributed to oxygen-metal bond, and the other fitted peaks at 531.14 and 532.04 eV are attributed to oxygen in hydroxide group, and a surface-adsorbed water molecule.

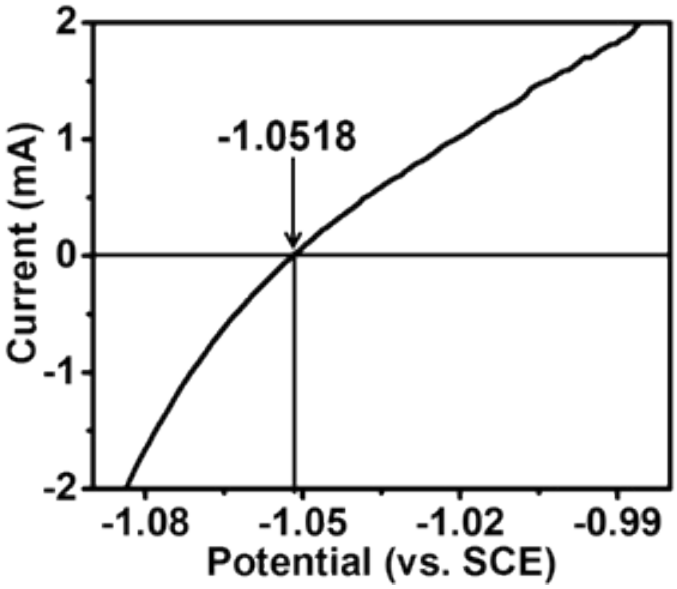

Fig. S19 RHE calibration. We used saturated calomel electrode (SHE) as the reference electrode in measurement. It was calibrated with respect to reversible hydrogen electrode (RHE). The calibration was performed in the high purity hydrogen saturated electrolyte with Pt wire as the working electrode. LSV were run at a scan rate of 1 mV s^{-1}, and potential at zero mA current, was taken to be the thermodynamic potential for hydrogen evolution reactions. So, in 1M KOH, E(RHE) = E(SCE) + 1.0518.

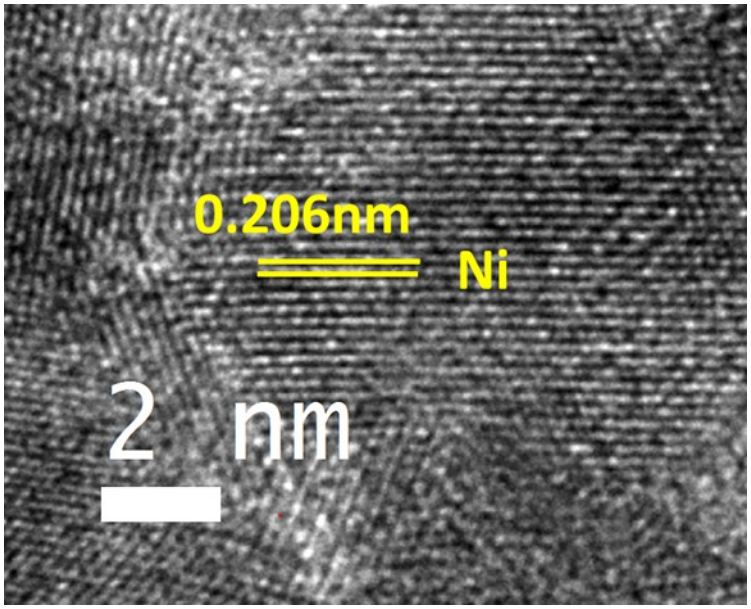

Fig. S20 The HRTEM images of V_2O_5/$Ni(OH)_2$@NF

Table S1. Atomic percent composition of various elements in V_2O_5/Ni(OH)$_2$@NF sample determined from XPS analysis.

Element	Atomic %
O1s	27.29
Ni2p$_3$	14.54
V2p	10.91

Table S2. Overpotentials of recently developed highly active non-novel metal catalysts.

	Overpotential at 10mA/cm^2 (mV)	Conditions (Electrolyte, Scan Rate, Gas Used)	Refs.
V_2O_5/Ni(OH)$_2$@NF	39	1M KOH	This work
20% Pt/C@NF	35	1M KOH	This work
VOOH Hollow Nanospheres	164	1M KOH	[1]
Pt NWs/SL-Ni(OH)$_2$	98 mV @5mA/cm^2	1 M KOH	[2]
Nanocrystalline Ni_5P_4	50	1M KOH	[3]
NiSe/NF	96	1M KOH	[4]
MoC_x nano-octahedrons	151	1M KOH	[5]
$NiCo_2Px$/CF	58	1 M KOH	[6]
NiO/Ni-CNT	80	1M KOH,	[7]
np(Co052Fe0.48)2P	79	1M KOH	[8]
Mn-CoP/Ti	76	1M KOH	[9]
$Zn_{0.30}Co_{2.70}S_4$	85	1M KOH	[10]
$(CoP)_{0.54}$-$(FeP)_{0.46}$-NRs/G	98	1M KOH	[11]
c-$CoSe_2$	200	1M KOH	[12]
Co-P/Cu foil	94	1M KOH	[13]
N, P-doped Mo_2C@carbon nanospheres	47	1M KOH	[14]
WC nanocrystals/CNTs	150	0.1M KOH	[15]
Cu NDs/Ni_3S_2 NTs-CFs	128	1M KOH	[16]
$Ni_{0.89}Co_{0.11}Se_2$ MNSN/NF	85	1M KOH	[17]
$NiFeO_x$/CFP	88	1M KOH	[18]
CoN_x/C	170	0.1M KOH	[19]
np-CuTi	47	0.1M KOH	[20]
Ni_3N@CQDs	69	1M KOH	[21]
W-SAC	53	0.1M KOH	[22]
N-doped Ni_3S_2	155	1M KOH	[23]
N–$NiCo_2S_4$	41	1M KOH	[24]
Co-Ex-MoS_2	89	1M KOH	[25]
MoP nanosheets	49	1M KOH	[26]
20% Pt/C@NF(1 mg)	31	1M KOH	[27]

References

1. H. Shi, H. Liang, F. Ming and Z. Wang, *Angew. Chem. Int. Ed.*, 2017, **56**, 573-577.
2. H. Yin, S. Zhao, K. Zhao, A. Muqsit, H. Tang, L. Chang, H. Zhao, Y. Gao and Z. Tang, *Nat. Commun.*, 2015, **6**, 6430.
3. A. B. Laursen, K. R. Patraju, M. J. Whitaker, M. Retuerto, T. Sarkar, N. Yao, K. V. Ramanujachary, M. Greenblatt and G. C. Dismukes, *Energ. Environ. Sci.*, 2015, **8**, 1027-1034.
4. C. Tang, N. Cheng, Z. Pu, W. Xing and X. Sun, *Angew. Chem. Int. Ed.*, 2015, **54**, 9351-9355.
5. H. B. Wu, B. Y. Xia, L. Yu, X.-Y. Yu and X. W. Lou, *Nat. Commun.*, 2015, **6**, 6512.
6. R. Zhang, X. Wang, S. Yu, T. Wen, X. Zhu, F. Yang, X. Sun, X. Wang and W. Hu, *Adv.Mater*, 2017, **29**, 1605502-n/a.
7. M. Gong, W. Zhou, M.-C. Tsai, J. Zhou, M. Guan, M.-C. Lin, B. Zhang, Y. Hu, D.-Y. Wang, J. Yang, S. J. Pennycook, B.-J. Hwang and H. Dai, *Nat. Commun.*, 2014, **5**, 4695.
8. Y. Tan, H. Wang, P. Liu, Y. Shen, C. Cheng, A. Hirata, T. Fujita, Z. Tang and M. Chen, *Energ. Environ. Sci.*, 2016, **9**, 2257-2261.
9. T. Liu, X. Ma, D. Liu, S. Hao, G. Du, Y. Ma, A. M. Asiri, X. Sun and L. Chen, *ACS. Catal.*, 2017, **7**, 98-102.
10. Z.-F. Huang, J. Song, K. Li, M. Tahir, Y.-T. Wang, L. Pan, L. Wang, X. Zhang and J.-J. Zou, *J. Am. Chem. Soc*, 2016, **138**, 1359-1365.
11. B. Liu, L. Huo, Z. Gao, G. Zhi, G. Zhang and J. Zhang, *Small*, 2017, **13**, 1700092-n/a.
12. P. Chen, K. Xu, S. Tao, T. Zhou, Y. Tong, H. Ding, L. Zhang, W. Chu, C. Wu and Y. Xie, *Adv.Mater*, 2016, **28**, 7527-7532.
13. N. Jiang, B. You, M. Sheng and Y. Sun, *Angew. Chem. Int. Ed.*, 2015, **54**, 6251-6254.
14. Y.-Y. Chen, Y. Zhang, W.-J. Jiang, X. Zhang, Z. Dai, L.-J. Wan and J.-S. Hu, *ACS Nano*, 2016, **10**, 8851-8860.
15. X. Fan, H. Zhou and X. Guo, *ACS Nano*, 2015, **9**, 5125-5134.
16. J.-X. Feng, J.-Q. Wu, Y.-X. Tong and G.-R. Li, *J. Am. Chem. Soc*, 2018, **140**, 610-617.
17. B. Liu, Y.-F. Zhao, H.-Q. Peng, Z.-Y. Zhang, C.-K. Sit, M.-F. Yuen, T.-R. Zhang, C.-S. Lee and W.-J. Zhang, *Adv.Mater*, 2017, **29**, 1606521-n/a.
18. H. Wang, H.-W. Lee, Y. Deng, Z. Lu, P.-C. Hsu, Y. Liu, D. Lin and Y. Cui, *Nat. Commun.*, 2015, **6**, 7261.
19. H.-W. Liang, S. Brüller, R. Dong, J. Zhang, X. Feng and K. Müllen, *Nat. Commun.*, 2015, **6**, 7992.
20. Q. Lu, G. S. Hutchings, W. Yu, Y. Zhou, R. V. Forest, R. Tao, J. Rosen, B. T. Yonemoto, Z. Cao, H. Zheng, J. Q. Xiao, F. Jiao and J. G. Chen, *Nat. Commun.*, 2015, **6**, 6567.
21. M. Zhou, Q. Weng, Z. I. Popov, Y. Yang, L. Y. Antipina, P. B. Sorokin, X. Wang, Y. Bando and D. Golberg, *ACS Nano*, 2018, **12**, 4148-4155.
22. W. Chen, J. Pei, C. T. He, J. Wan, H. Ren, Y. Wang, J. Dong, K. Wu, W. C. Cheong and J. Mao, *Adv.Mater*, 2018, **30**, 1800396.
23. T. Kou, T. Smart, B. Yao, I. Chen, D. Thota, Y. Ping and Y. Li, *Adv. Ener. Mater.*, 2018, **8**, 1703538.
24. Y. Wu, X. Liu, D. Han, X. Song, L. Shi, Y. Song, S. Niu, Y. Xie, J. Cai, S. Wu, J. Kang, J. Zhou, Z. Chen, X. Zheng, X. Xiao and G. Wang, *Nat. Commun.*, 2018, **9**, 1425.
25. Y. Luo, X. Li, X. Cai, X. Zou, F. Kang, H.-M. Cheng and B. Liu, *ACS Nano*, 2018, **12**, 4565-4573.
26. G. Li, Y. Sun, J. Rao, J. Wu, A. Kumar, Q. N. Xu, C. Fu, E. Liu, G. R. Blake, P. Werner, B. Shao, K. Liu, S. Parkin, X. Liu, M. Fahlman, S.-C. Liou, G. Auffermann, J. Zhang, C. Felser and X. Feng, *Adv. Ener. Mater.*, 2018, **8**, 1801258.
27. B. Liu, Y.-F. Zhao, H.-Q. Peng, Z.-Y. Zhang, C.-K. Sit, M.-F. Yuen, T.-R. Zhang, C.-S. Lee and W.-J. Zhang, *Adv.Mater*, 2017, **29**, 1606521.